1993

Comparison of the cosmic microwave and cosmic x-ray backgrounds: constraints on local sources of the fluctuations observed by COBE

Stephen P. Boughn
Haverford College, sboughn@haverford.edu

K. Jahoda

THE ASTROPHYSICAL JOURNAL, 412:L1–L4, 1993 July 20

A COMPARISON OF THE COSMIC MICROWAVE AND COSMIC X-RAY BACKGROUNDS: CONSTRAINTS ON LOCAL SOURCES OF THE FLUCTUATIONS OBSERVED BY *COBE*

S. P. BOUGHN
Department of Astronomy, Haverford College, Haverford, PA 19041
AND
K. JAHODA
NASA/Goddard Space Flight Center, Code 666, Greenbelt, MD 20771
Received 1993 March 8; accepted 1993 May 3

ABSTRACT

It has been suggested by Hogan (1992) that the microwave background anisotropy detected by the *COBE* DMR experiment (Smoot et al. 1992) might be produced by inverse Compton scattering from hot diffuse clouds of electrons in nearby superclusters. If the *COBE* fluctuations are due to this mechanism, then the absence of anticorrelations between maps of the cosmic microwave and cosmic X-ray backgrounds constrains the temperature ($kT_e > 16$ keV) and density ($n_e < 2 \times 10^{-6}$ cm^{-3}) of the ionized supercluster gas. Since the *COBE* limits on spectral distortion indicate that the temperature of the intergalactic medium is less than 10 keV, we conclude that the fluctuations observed by *COBE* are probably not produced by this mechanism.

Subject headings: cosmic microwave background — cosmology: observations — intergalactic medium — X-rays: general

1. INTRODUCTION

The intermediate-scale (10°) anisotropy in the cosmic microwave background (CMB) observed by the *COBE* satellite has been interpreted as resulting from density fluctuations at the epoch of recombination, i.e., $z \sim 1000$ (Wright et al. 1992). Hogan (1992) suggested that this anisotropy might, on the other hand, be dominated by scattering from hot electrons in optically thin, nearby superclusters, i.e., the Sunyaev-Zel'dovich (S-Z) effect (Sunyaev & Zel'dovich 1980). Bremsstrahlung from such electrons would also contribute to the fluctuations in the cosmic X-ray background (CXB). Furthermore, these fluctuations would be anticorrelated with CMB fluctuations since the S-Z effect results in a decrement in the CMB on the Rayleigh-Jeans side of the spectrum. This *Letter* reports the results of an attempt to observe this effect by cross-correlating a full sky map of the CMB with one of the CXB. If the structure in the *COBE* maps is, indeed, due to the S-Z effect, then one would expect the cross-correlation function to show the same sort of structure as the *COBE* maps on an angular scale of 10° but with a negative sign. The amplitude depends on the temperature, density, size, and distribution of the supercluster pancakes.

The CMB temperature decrement for radiation passing through a gas cloud of uniform density N_e, thickness L, and temperature T_e is given by (Hogan 1992)

$$(\delta T/T)_{\rm CMB} = -7.8 \times 10^{-6} l n_e t_e \,, \tag{1}$$

where $l = L/30$ Mpc, $n_e = N_e/10^{-5.5}$ cm^{-3}, and $t_e = kT_e/10$ keV. On the other hand, the X-ray intensity due to bremsstrahlung in the cloud is (Daly 1992)

$$I = 3.4 \times 10^{-9} l n_e^2 t_e^{1/2} \ (\text{ergs s}^{-1}\ \text{cm}^{-2}\ \text{sr}^{-1}) \,. \tag{2}$$

The cross-correlation function is defined by $C_{TI}(\theta) = \langle \delta T\, \delta I \rangle$ which is the average product of the CMB and CXB fluctuations in directions separated by an angle, θ. Equations (1) and (2) can be used to express $C_{TI}(\theta)$ in terms of model parameters, i.e.,

$$C_{TI}(\theta) = -7.3 \times 10^{-14} f(\theta) l^2 n_e^3 t_e^{3/2} \ (\text{K ergs s}^{-1}\ \text{cm}^{-2}\ \text{sr}^{-1}) \,, \tag{3}$$

where $f(\theta)$ is a dimensionless factor that depends on the density and distribution of supercluster pancakes and $T_{\rm CMB} = 2.73$ K. It should be noted that the strength of the signal is fairly sensitive to the model parameters l, n_e, t, and $f(\theta)$. A much more stringent test of the model is provided by a direct comparison with the fluctuations observed by *COBE*. If the supercluster gas is responsible for the structure observed by *COBE*, then the autocorrelation function of the fluctuations in the CMB is

$$C_T(\theta) = 4.5 \times 10^{-10} f(\theta) l^2 n_e^2 t_e^2 \ (\text{K}^2) \,. \tag{4}$$

Note that the angular dependences in $C_{TI}(\theta)$ and $C_T(\theta)$ are exactly the same only for uniform density gas. On the other hand, if the gas is clumped, then X-ray luminosity is increased; and the constraints on the model parameters which appear below become stronger. The ratio of the cross-correlation and autocorrelation functions is

$$C_{TI}(\theta)/C_T(\theta) = 1.6 \times 10^{-4} n_e t_e^{-1/2} \ (\text{ergs s}^{-1}\ \text{cm}^{-2}\ \text{sr}^{-1}\ \text{K}^{-1}) \,. \tag{5}$$

This expression does not depend on the sizes and distribution function of the superclusters and is much less sensitive to model parameters n_e and t. Finally, a comparison of the autocorrelation functions of the two maps also provides significant constraints on the model parameters. From equations (1) and (2) it is clear that

$$\sqrt{C_I(\theta)/C_T(\theta)} \geq 1.6 \times 10^{-4} n_e t_e^{-1/2} \ (\text{ergs s}^{-1}\ \text{cm}^{-2}\ \text{sr}^{-1}\ \text{K}^{-1}) \,, \tag{6}$$

where $C_I(\theta)$ is the autocorrelation function of the X-ray background. Notice that the right-hand sides of equations (5) and (6) are the same, but the former involves the cross-correlation function, $C_{TI}(\theta)$, while the latter uses the X-ray autocorrelation function, $C_I(\theta)$. Also, equation (6) is an inequality since the CXB autocorrelation function may well involve contributions that are not correlated with the CMB.

2. CMB AND CXB MAPS

The microwave and X-ray data used in this analysis were provided by the 19 GHz map of Boughn et al. (1992) and the nominal 2–60 keV map of the A-2 experiment aboard the *HEAO 1* satellite (Boldt 1987). The angular resolution of both of these maps is about 3°, compared to the 7° beam width of the *COBE* antennas.

Although both of the data sets comprised full sky maps, more than half of the data were removed before the analysis. The dominant feature in both maps is the plane of the Galaxy, so all data within 20° of the Galactic plane were cut. Data within 30° of the Galactic center and within 10° of Orion were also excluded, since these features were both visible in the 19 GHz map. These cuts, combined with two small regions near the celestial poles which were not observed in the 19 GHz map, correspond to 39% of the data. In addition, 10° diameter regions around 90 discrete X-ray sources (Piccinotti et al. 1982) were removed. Finally, the X-ray map itself was searched for weak point "sources" that exceed the nearby background by 9 σ, and 7° diameter regions around them were removed. Thirty-nine such "sources" were found. Together these "source" cuts accounted for 19% of the initial data set. Therefore, the final "cleaned" maps were reduced to 42% of full sky coverage.

2.1. *HEAO 1 A-2 X-Ray Map*

The *HEAO 1* A-2 experiment was designed to measure surface brightness in the 0.1–60 keV X-ray band (Rothschild et al. 1979; Boldt 1987). The present analysis was from two medium-energy detectors (MED) with different fields of view (3° × 1°.5 FWHM and 3° × 3° FWHM) and two high-energy detectors (HED3) with the same fields of view. Counts from these detectors were combined and binned in 1°.3 × 1°.3 pixels on the sky, i.e., the map was slightly overresolved. The combined map had sensitivity from 2 to 60 keV and quantum efficiency over 50% between 3 and 17 keV (Jahoda & Mushotzky 1989).

The data were collected by scanning great circles along lines of constant ecliptic longitude. The experiment performed one complete revolution every 33 minutes, with the spin axis pointed at the Sun. All data used in this analysis were collected during the 6 month period beginning on day 322 of 1977. When plotted as a function of time, the data showed a slight linear drift of unknown origin which was fitted for and subsequently removed from the map.

In order to check for a high-latitude ($|b| > 20°$) Galactic contribution, the X-ray map was fitted to both a Galaxy secant law and to the synchrotron map of Haslam et al. (1982). Both fits were statistically significant; however, the latter was a better fit so was used to correct the X-ray map for Galactic emission. The results of this *Letter* are independent of whether or not this final correction was made.

2.2. 19 GHz *Map*

The 19 GHz map is considerably noisier than the *COBE* DMR maps. The average rms noise per 3° resolution element is 0.8 mK. In addition, the coverage was not uniform, so the noise varied considerably over the sky. A weighted least-squares fit to a dipole gave a value consistent with other measurements, including that found by *COBE*. The fit dipole was removed from the map. In addition, a high-latitude Galactic contribution was estimated, as in the case of the X-ray map, by fitting to the Haslam synchrotron map. The fit component was subsequently subtracted from the 19 GHz map. Correcting both the X-ray and 19 GHz maps with the same synchrotron map can potentially introduce spurious correlations between the two which are not actually present in the two maps; however, the results presented below do not depend on these corrections.

3. CORRELATION ANALYSIS

In order to constrain model parameters using equations (5) and (6), the autocorrelation function of the CXB, $C_I(\theta)$, and the cross-correlation function of the CMB and CXB, $C_{TI}(\theta)$, had to be estimated. The CMB autocorrelation function is taken to be that found by *COBE* (Smoot et al. 1992). To obtain these estimates, the two maps were rebinned into 2°.6 × 2°.6 pixels, the same resolution as used in the *COBE* analysis. The X-ray autocorrelation function was then taken to be

$$C_I(\theta) = \sum_{j,k/\theta} (\Delta I_j \Delta I_k) \Big/ \sum_{j,k/\theta} 1 , \qquad (7)$$

where $\Delta I_j = (I_j - \langle I \rangle)$, the summation is over the intensities of all pixel pairs, j and k, separated by an angle θ. Because of uneven coverage in the CXB map, the measurement noise per pixel (shot noise) was not uniform across the sky. However, the fluctuations in the CXB map on every angular scale are significantly larger than this noise. It, therefore, seemed prudent not to weight the terms of the sum inversely with the noise variances as is usually the case. Figure 1 is a plot of $C_I(\theta)$. The error bars are computed from the shot noise alone in the absence of correlated signal. It is clear from the figure that even after the cleaning procedure described above there is a great deal of correlated structure in the map. The details of the shape of the correlation function depend on how much and by what method the data are cleaned; however, using a different set of selection criteria, Jahoda (1992) found similar structure for $\theta < 20°$.

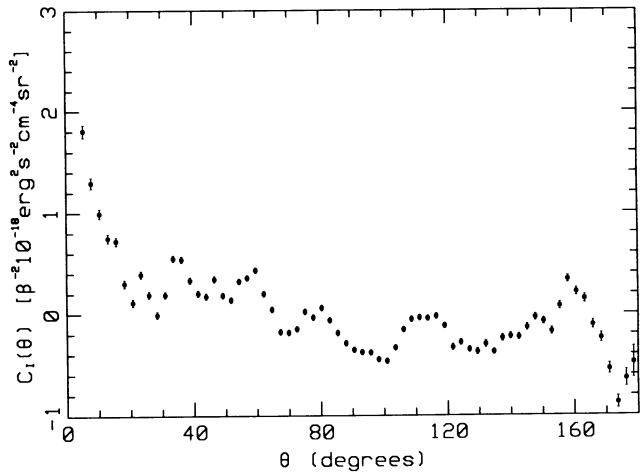

FIG. 1.—Autocorrelation function of the *HEAO 1* A-2 X-ray map. β is a dimensionless parameter that depends on the spectrum. For a 10 keV bremsstrahlung spectrum, $\beta = 1$. Error bars represent shot noise.

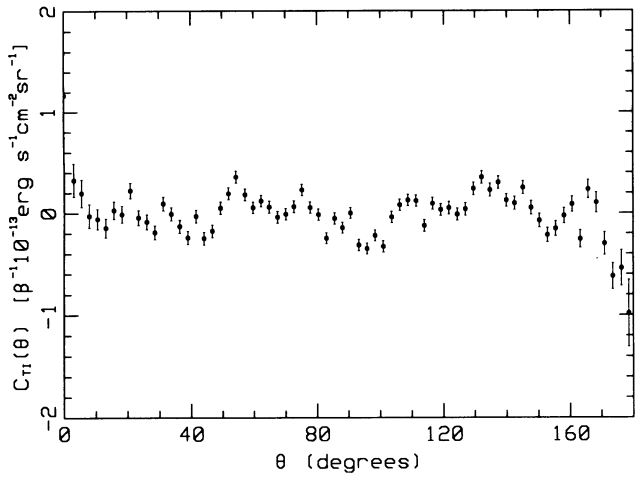

FIG. 2.—Cross-correlation function of the *HEAO 1* A-2 X-ray and 19 GHz maps. β is the same parameter as in Fig. 1. The error bars represent uncorrelated, statistical noise only.

The cross-correlation function is given by

$$C_{TI}(\theta) = \sum_{j,k/\theta} \Delta T_j \Delta I_k / \sigma_j^2 \Big/ \sum_{j,k/\theta} 1/\sigma_j^2 , \quad (8)$$

where the sum is over the CMB temperature, ΔT_j, and the CXB intensity, ΔI_k, of pixels separated by an angle θ and σ_j^2 is the noise variance of the jth pixel of the CMB map. Unlike the CXB map, the 19 GHz CMB map is dominated by noise so the terms in the sum are weighted inversely with the variances of the pixels of the CMB map. Figure 2 is a plot of $C_{TI}(\theta)$. The error bars were computed from the measurement noises in the two maps, assuming no structure in either map. As a consequence of the structure in the X-ray map (see Fig. 1), the largest contribution to the error in the cross-correlation function results from the measurement errors in the CMB map multiplied by the real structure of the CXB map. The resulting errors at each θ are difficult to compute directly and are not independent of each other. A Monte Carlo investigation of these errors was conducted by cross-correlating the real CXB map with a series of fake CMB maps generated to be consistent with the measurement noise alone. The resulting correlation functions were similar to Figure 2 but, of course, with the peaks and valleys at different places. We conclude that the structure in Figure 2 is consistent with noise.

4. CONSTRAINTS ON THE S-Z MODEL

Similar structure is observed in the cross-correlation function of the *COBE* DMR 53 GHz and 90 GHz maps and the autocorrelation function of the 53 GHz map (Smoot et al. 1992). At small angular scales ($<20°$), this structure can be reasonably well fitted by a linear function with $C_T(0) = 900$ μK^2 and $C_T(20°) = 0$. If the S-Z hypothesis for the CMB fluctuations is true, then one would expect the signal at 19 GHz to be slightly stronger than at the *COBE* DMR frequencies since the Compton Y-parameter is slightly less at the higher frequencies. Taking this factor into account, at 19 GHz one would expect $C_T(0) = 1200$ μK^2. According to Hogan's S-Z model for the CMB fluctuations, there should appear similar structure in the autocorrelation of the CXB and in the cross-correlation of the CXB and CMB (with negative correlations in the case of the latter). In fact, Figure 1 does show such a linear structure with amplitude

$$C_I(0) = 2.3 \times 10^{-18} \beta^2 \text{ (ergs}^2 \text{ s}^{-2} \text{ cm}^{-4} \text{ sr}^{-2}) ,$$

where β is a dimensionless factor that depends on the shape of the passband and on the bremsstrahlung spectrum, i.e., on kT_e. The normalization is such that $\beta = 1$ for $kT_e = 10$ keV. Substituting this value and the value for $C_T(0)$ into equation (6) yields a constraint on the model parameters n_e and t of $\beta n_e t_e^{-1/2} < 0.27$. Only an upper limit can be provided by this analysis since there is no evidence that the structure in the two maps is correlated.

On the other hand, the cross-correlation function of Figure 2 does not reveal the expected structure and, therefore, also only provides a constraint on the model parameters. A linear function was fit in the region $0° \le \theta \le 20°$ with the constraint that it vanish at $\theta = 20°$. The amplitude of the fit was

$$C_{TI}(0) = 1.2 \pm 3.5 \times 10^{-14} \beta \text{ (K ergs s}^{-1} \text{ cm}^{-2} \text{ sr}^{-1}) .$$

The error in the fit was determined from the scatter in fits to 100 Monte Carlo trials in which the true X-ray map was cross-correlated with a map of random noise consistent with that of the 19 GHz map. The resulting 90% confidence level upper limit to the amplitude is

$$C_{TI}(0) < 4.4 \times 10^{-14} \beta \text{ (K ergs s}^{-1} \text{ cm}^{-2} \text{ sr}^{-1}) .$$

This value was checked by another Monte Carlo test in which random but correlated structure of this amplitude was added to both the true X-ray map and to simulated 19 GHz maps. A linear fit to the resulting cross-correlation functions resulted in the expected amplitude with the scatter consistent with that quoted above. Substituting this value for $C_T(0)$ into equation (5) results in another constraint on model parameters, i.e., $\beta n_e t_e^{-1/2} < 0.23$, which is slightly stronger than the constraint above.

Since β is a rather complicated function of a gas temperature, T_e, the constraints on N_e and T_e are graphically represented in Figure 3. The hatched region of parameter space is excluded at the 90% confidence level. The constraints on N_e and T_e together with equation (4) imply similar constraints on supercluster parameters f and L. These are graphically represented in Figure 4 where it is assumed that $C_T(0) = 1200$

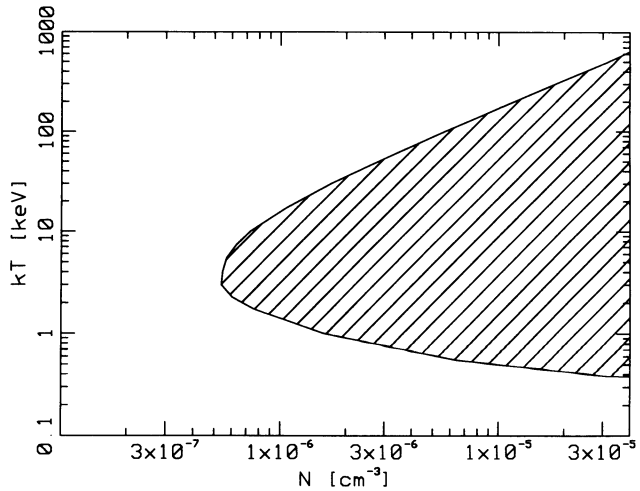

FIG. 3.—Limits on model parameters N_e and T_e. The hatched area is excluded at the 90% confidence level.

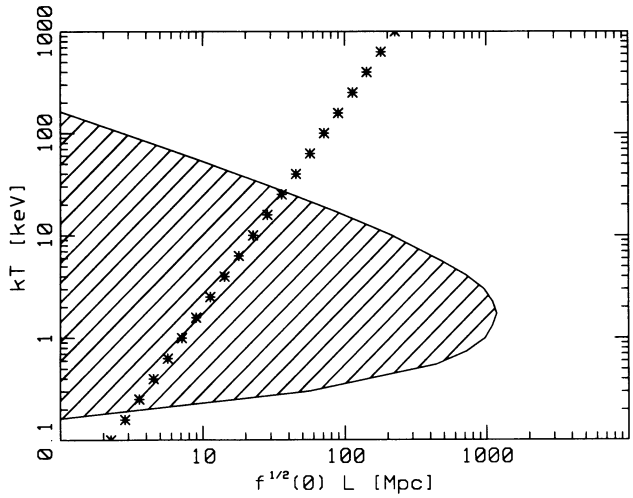

FIG. 4.—Limits on model parameters $f(0)^{1/2}L$ and T_e. The hatched area is excluded at the 90% level. The starred line is the temperature corresponding to a velocity $H_0 L$ (see text).

μK^2. The hatched region is excluded at the 90% confidence level.

The starred line represents the temperature corresponding to the velocity $H_0 L$ where the Hubble constant H_0 has been assumed to be 75 km s^{-1} Mpc^{-1}. For a given L [note we have assumed $f(0) \sim 1$], it represents roughly the energy per particle available to heat the gas. Of course, the gas temperature depends on the details of supercluster collapse so this curve can be considered only as an approximate upper limit on the temperature. Then Figure 4 implies that only large structures, i.e., $f(0)^{1/2}L \gtrsim 40$ Mpc, can account for the *COBE* fluctuations unless the gas temperature is quite low, i.e., $kT_e \lesssim 0.3$ keV.

If one assumes that it is unlikely for the supercluster length scale to be larger than 100 Mpc, then Figure 4 also implies that either $kT_e < 0.35$ keV or $kT_e > 16$ keV. The former can be ruled out since the density required to account for the *COBE* fluctuations (see eq. [4]) is so large that the resulting bremsstrahlung emission far exceeds the soft X-ray background (McCammon & Sanders 1990). On the other hand if $kT_e > 16$ keV and $f(0)^{1/2}L > 40$ Mpc, then equation (4) implies that the supercluster gas must be relatively diffuse, i.e., $N_e < 2 \times 10^{-6}$ cm^{-3}.

The "sources" cleaning procedure described above resulted in 19% of the data being cut from the maps. If these point sources are actually responsible for the signal observed by *COBE*, then the cross-correlation signal would have been eliminated by the cleaning procedure and the constraints invalid. To check for this possibility, the mean square signals for these pixels in the 19 GHz were computed and found to be -900 ± 625 μK^2. Since the angular resolution of the 19 GHz map was $\frac{3}{7}$ that of the *COBE* maps, such point sources would be 5.4 times stronger in the 19 GHz map. In addition, since the "source" pixels comprised only 25% of those pixels in the *COBE* analysis, the mean square average over these pixels would be 4 times larger than when averaged over all pixels. Therefore, one would expect the mean square signal over the source pixels to be 25 times larger than the value of $C_T(0)$ found by *COBE* where the difference in Compton Y-parameters was again taken into account. A comparison of these two values clearly indicates that the X-ray sources are not the source of the *COBE* fluctuations.

4. CONCLUSION

The lack of correlation between the *HEAO 1* A-2 X-ray map and the 19 GHz microwave map constrains models of hot, intergalactic gas that have been suggested as a possible explanation for the fluctuations observed by *COBE*. These constraints are represented graphically in Figures 3 and 4. Of the remaining parameter space available, the most "reasonable" model consists of a hot ($kT_e > 16$ keV), diffuse ($N_e > 2 \times 10^{-6}$ cm^{-3}) supercluster gas. Wright et al. (1993) have argued that lack of spectral distortion of the CMB implies an upper limit of 10 keV for the temperature of the intergalactic medium. We conclude that it is unlikely that fluctuations observed by *COBE* are due to the S-Z effect in superclusters.

Whether or not some small fraction of the *COBE* fluctuations is due to this effect has not been ruled out. A direct comparison of the 53 GHz *COBE* map with the *HEAO 1* A-2 map should be sensitive to an inverse Compton component at the level of about 0.1 of the *COBE* fluctuations. The detection of a signal at this level would provide important information about the intergalactic medium.

We would like to thank Ruth Daly for many helpful discussions regarding this work; David Cottingham, Ed Cheng, and Dale Fixsen for their work on the 19 GHz map; and Craig Hogan for several helpful suggestions. We also acknowledge Ken Ganga, Lyman Page, Jon Marr, and Tom Evans for helpful conversations. This work was supported in part by NASA grant NAF 5-1713 and NSF grant AST-8914988.

REFERENCES

Boldt, E. 1987, Phys. Rep., 146, 215
Boughn, S. P., Cheng, E. S., Cottingham, D. A., & Fixsen, D. J. 1992, ApJ, 391, L49
Daly, R. A. 1992, ApJ, 399, 426
Haslam, C. G. T., Salter, C. J., Stoffel, H., & Wilson, W. E. 1982, A&AS, 47, 1
Hogan, C. 1992, ApJ, 398, L77
Jahoda, K. 1992, in Recent Results in X-Ray and EUV Astronomy (COSPAR Symp.), ed. J. Trümper, in press
Jahoda, K., & Mushotzky, R. F. 1989, ApJ, 346, 638,
McCammon, D., & Sanders, W. T. 1990 ARA&A, 28, 657
Piccinotti, G., Mushotzky, R. F., Boldt, E. A., Holt, S. S., Marshall, F. E., Serlemitsos, P. J., & Shafer, R. A. 1982, ApJ, 253, 485
Rothschild, R., et al. 1979, Space Sci. Instr., 4, 265
Smoot, G., et al. 1992, ApJ, 396, L1
Sunyaev, R. A., & Zel'dovich, Ya. B. 1980, ARA&A, 18, 537
Wright, E. L., et al. 1992, ApJ, 396, L13
Wright, E. L., et al. 1993, ApJ, submitted